Characterization of Randomly Branched Poly(vinylidene fluoride)

Lotfi Hedhli,* Nafaa Mekhilef, Stephane Moyses, and Russell H. Lewis

Arkema Inc., Technical Research Center, 900 First Avenue, King of Prussia, Pennsylvania 19406

Received May 23, 2007; Revised Manuscript Received December 18, 2007

ABSTRACT: Poly(vinylidene fluoride) (PVDF) experimental samples containing sparsely distributed chain branching were compared to commercial reference samples. The results showed a lower onset of shear thinning for the branched samples over the reference counterparts. The storage modulus of the branched samples at low frequency shows a significant increase for the low-molecular weight sample while the higher-molecular weight sample showed a moderate increase suggesting a strong contribution of chain branching. The branched PVDF samples exhibited a lower radius of gyration (R_G) and intrinsic viscosity than the commercial samples over the entire molecular weight range. NMR revealed the presence of tertiary carbons, suggesting that the branches are covalently bonded and not of a physical nature. Extensional viscosity data showed that the branched samples display a significant degree of strain hardening while the reference samples exhibit a small degree of strain hardening.

Introduction

The performance of polymers during processing is essentially dominated by their viscoelastic properties, which, in turn, are dependent on the molecular structure. Properties such as molecular weight (MW) and molecular weight distribution (MWD) are known to affect the melt viscosity, shear thinning, and creep and recoverable compliance. Additionally, long chain branching (LCB) is also known to produce dramatic effects on the rheological properties such as a lower onset of shear thinning than linear counterparts and an increased die swell. The combination of all three parameters (MW, MWD, and LCB) constitutes the essence of molecular structure−rheology relationships in polymers. When properly controlled, these parameters offer multiple rheological properties suitable for a variety of polymer processes. One approach to achieve a balance of properties is to introduce a controlled number and length of long chain branches into the main backbone of the polymer. This allows for a wide range of architectures and hence widens the range of melt rheological properties.[1−4] Several technologies have been devised to produce long chain branching such as stars, combs, or dendrimers.[5,6] In olefin polymerization, catalysts are used to create controlled LCB containing polyethylene by copolymerization of ethylene with higher α-olefins[7] for condensation polymers, multifunctional monomers, or branched diacids[8,9] are used to create LCB. Another route to introduce LCB is to use macromononers.[10]

While there has been extensive work and research done on the synthesis of branched polypropylene and polyethylene, there has been a limited amount of work done in the area of engineering resins.[11−15] Fluoropolymers, an important class of engineering resins, find applications in three main areas: melt processing such as extrusion and injection molding, architectural coatings, and porous membranes produced by solvent casting. In melt processing, poly(vinylidene fluoride) (PVDF) exhibits a moderate shear-thinning behavior and low melt strength at low molecular weights, features characteristic of many linear polymers. Increasing the molecular weight only increases the viscosity and melt strength and decreases the draw-down ratio. It is therefore difficult to obtain a balance between the parameters of melt strength and draw-down ratio without chemically changing the structure of the polymer. Crosslinking via either chemical modification or radiation[16,17] may increase the melt strength, but the resulting polymers are limited in terms of processability and often contain a high amount of insoluble fraction. Recently, the introduction of LCB in a fluoropolymer has been achieved[17−19] by using a chain transfer mechanism based on iodine along with bifunctional molecules. Another approach to prepare fluoropolymers containing LCB has been proposed by others,[20] using a dehydrofluorinating agent thereby forming double bonds in the fluoropolymer backbone which are later used to cause branching of the fluoropolymer.

In the present paper, the properties and characterization of novel fluoropolymers containing LCB and prepared by an emulsion polymerization process are discussed. The polymers were also compared to reference samples prepared by a commercial process. The characterization protocol included small amplitude oscillatory measurements, extensional rheology, size exclusion chromatography in combination with light scattering (SEC/MALLS/online viscosity) and NMR to get further insight into the relationship between rheology and the topography of PVDF containing LCB.

Experimental Section

The reference samples PVDF 1−5 are commercially available from Arkema Inc. under the tradename Kynar and were produced by a conventional polymerization process in which a chain transfer agent is used to control the molecular weight. The samples selected cover a wide range of molecular weight while their polydispersity index remains almost identical.

Both *n*-butyl-4,4-bis(*tert*-butylperoxy) valerate (Luperox 230)- and di(*tert*-amyl) peroxide (Luperox DTA) were obtained from Arkema and used as received.

Figures 1 and 2 show the primary radical from the Luperox 230 initiator which leads to reactive species (methyl radical) and nonreactive species (e.g., acetone) via β scission.

For the experimental samples, the polymerization reactions have been carried out in a 8 L stainless steel reactor. Appropriate process review and safety precautions should be taken due to the high pressure involved in these experiments. Details concerning the polymerization are reported in a pending patent.[21] The general procedure is as follows: A mixture of 4300 g of water, 11 g of surfactant, 5−10 g of ethyl acetate, and Luperox 230 (1.7 g) was added to the reactor. The mixture was purged with argon and

* To whom correspondence should be addressed.

10.1021/ma071160z CCC: $40.75
Published on Web 03/01/2008

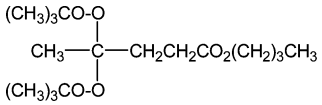

Figure 1. Chemical structure of Luperox 230.

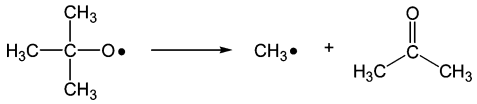

Figure 2. Scheme of β scission reaction in Luperox 230.

Table 1. Polymerization Conditions for the Branched PVDF Samples

	temperature (°C)	pressure (kPa)	agitator speed (rpm)	latex solids content (wt %)	reaction yield %
B-1	125	4600	90	22	90
B-2	125	4600	90	23	95
B-3	125	4600	90	20	92

Table 2. Melting Point (T_m) and Heat of Fusion (ΔH) for (a) Commercial Samples and (b) Branched PVDF Samples

properties	PVDF-1	PVDF-2	PVDF-4	B-1	B-2	B-3
T_m (°C)	167.0	169.4	168.8	163.1	162.9	162.5
ΔH (J/g)	56.1	55.8	55.8	50.3	53.3	49.9

Table 3. Molecular Weight Results Obtained by MALLS for the Commercial Samples

sample	PVDF-5	PVDF-1	PVDF-2	PVDF-3	PVDF-4
			MALLS		
$M_{w,SEC-LS}$ (g/mol)	110 000	118 000	162 000	189 000	255 000
$M_{z,SEC-LS}$ (g/mol)	205 000	217 000	334 000	397 000	567 000
M_z/M_w	1.9	1.8	2.1	2.1	2.2
$R_{G,w}$ (nm)	12.7	17.6	20.3	19.6	23.8
			PMMA Calibration		
M_w (g/mol)	200 000	213 000	276 000	311 000	398 000
M_n (g/mol)	108 000	116 000	139 000	145 000	169 000
M_w/M_n	1.9	1.8	2.0	2.1	2.4

agitated for 10 min. The reactor was sealed and heated to 125 °C under continuous agitation. The reactor was charged with vinylidene fluoride monomer to reach a pressure of 4600 kPa. A 1.6 wt % potassium persulfate solution was then fed continuously at an initial rate of about 100−120 g/h, then set at 60 g/h after 30 min. A constant reaction pressure was maintained by adding vinylidene fluoride as needed. After 2.5 h, the monomer feed was stopped and agitation and heating were continued for another 15 min. After cooling to room temperature, surplus gas was vented, and the reactor was discharged of latex through a stainless steel mesh. Gravimetric analysis showed the solid content to be 22 wt %. The samples were then dried in a convection oven at 110 °C overnight.

Three experimental branched PVDF samples B1−B3 discussed in this paper have been prepared following the general procedure given above, under the same experimental conditions except for ethyl acetate which was varied to control the molecular weight. Sample B-4 was prepared using a higher amount of Luperox coinitiator. The main characteristics of the samples prepared are shown in Tables 1−4.

SEC-MALLS-Viscosity. A comprehensive molecular weight characterization protocol was used to examine the reference and experimental samples. The chromatographic system used consisted of a Waters GPCV 2000 with a temperature-controlled column/detector compartment holding a three-capillary viscometer and a differential refractometer (DRI). The temperature in the column/detector compartment was maintained at 95 °C. The light scattering

Table 4. Molecular Weight Results Obtained by MALLS for the Branched Polymers

sample	B-4	B-1	B-2	B-3
		MALLS		
$M_{w,SEC-LS}$ (g/mol)	102 000	250 000	260 000	670 000
$M_{z,SEC-LS}$ (g/mol)	320 000	940 000	740 000	2 300 000
M_z/M_w	3.2	3.8	2.8	3.4
$R_{G,w}$ (nm)	14.3	16.3	18.9	32.7
		PMMA Calibration		
M_w (g/mol)	144 000	299 000	350 000	588 000
M_n (g/mol)	57 000	111 000	135 000	167 000
M_w/M_n	2.5	2.7	2.6	3.5

measurements were made using a high-temperature Dawn EOS multiangle light scattering instrument (Wyatt Technology). The flow cell and the lines connecting the light scattering detector to the columns and the refractometer were also held at 95 °C.

The data was acquired using ASTRA software from Wyatt. The AUX1 analog port of the EOS was used to read the DRI signal and the AUX2 port was used to read the relative viscosity η_{rel} directly from the I/O port of the GPCV 2000. The solutions were prepared at 2.0 mg/mL in dimethyl sulfoxide (DMSO) and filtered prior to injection with a 0.45 μm PTFE membrane filter. A set of two size exclusion columns (PLgel mixed B, 10 μm particle size, Polymer Laboratories) was used. For the data analysis, the following equations were used to calculate the molecular weight and the root-mean-square radius of gyration R_G for each elution slice

$$\frac{Kc}{I(q)} = \frac{1}{M_w P(q)} + 2A_2 c \tag{1}$$

$$\lim \left[\frac{1}{P(q)}\right]_{q\to 0} = 1 + \frac{q^2 R_G{}^2}{3} \tag{2}$$

$$\frac{Kc}{I(q)} = \frac{1}{M_w}\left(1 + \frac{R_G{}^2 q^2}{3}\right) + 2A_2 c \tag{3}$$

where $I(q)$ is the excess Rayleigh scattering ratio (cm^{-1}), $P(q)$ is the form factor of the particle of molecular weight M_w, and K is a constant given for vertically polarized light, $K = 4\pi^2 n^2 (dn/dc)^2/N_A\lambda^4$, where n is the index of refraction of the pure solvent (DMSO), λ the wavelength of the incident light, N_A is Avogadro's number, and dn/dc is the differential refractive index of the polymer in the pure solvent. The magnitude of the scattering vector q is defined by $q = (4\pi n/\lambda)\sin(\theta/2)$, where θ is the angle at which scattered light is measured. Equation 3 is valid when $q^2R_G{}^2 \ll 1$. Under normal chromatographic conditions, the second term of the right-hand side of eq 3 is negligible. With the use of the data of Tsierkezos et al.,[22] the temperature coefficient of the refractive index is 4.75×10^{-4} K^{-1} at 589 nm. With the use of this value, the refractive index of DMSO at 95 °C $n^{95\ °C} = 1.444$ is obtained.

The differential refractometer and the light scattering detector operate at different wavelengths (880 and 690 nm, respectively). However there is only a small dependence of the differential refractive index with wavelength.[23] For example, there is a 3% difference between the differential refractive index of PVDF in DMSO measured at 545 and 632 nm.[24] The temperature dependence of the differential refractive index is determined by the temperature dependence of the refractive index of the solvent and the polymer. Lutringer et al.[24] measured the differential refractive index of PVDF in a variety of solvents. In DMSO, they reported $dn/dc = -0.060$ mL/g at 632 nm and 25 °C. We measured the differential refractive index of PVDF in DMSO at different temperatures. The results of which are shown in Figure 3. Our measurement carried out at 95 °C yields a dn/dc of −0.05 mL/g. The absolute value of the refractive index increment of PVDF in DMSO decreases linearly with the temperature in the range of 25−95 °C. This means that as the temperature increases, the contrast between the polymer and the solvent decreases, and the contribution of the polymer to the scattered light decreases. On the other hand, as the temperature

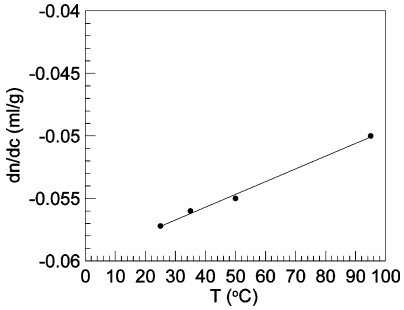

Figure 3. Differential refractive index increment d*n*/d*c* measured for PVDF-5 in DMSO as a function of temperature ($\lambda = 880$ nm).

increases, the radius of gyration of the polymer increases because of the swelling of the coil, which makes it possible to determine the radius of gyration for shorter polymer chains.

The instrument and procedure were validated using a set of poly(methyl methacrylate) (PMMA) standards with narrow polydispersity index. The molecular weights obtained in DMSO were in excellent agreement with the numbers obtained in THF.

The intrinsic viscosity, $[\eta]$, is obtained from the equation

$$\frac{\eta - \eta_S}{\eta_S c} = [\eta](1 + k_H[\eta]c + ...) \quad (4)$$

where η and η_S are the solution and solvent viscosities, respectively, and k_H is the Huggins coefficient. For dilute solutions, such as in the case of SEC, the left-hand side of eq 4 is a good approximation of $[\eta]$.

NMR. Sample solutions were prepared for ^{13}C NMR by dissolving the samples in DMSO-d_6 at 80 °C to make an approximate final concentration of 30% by volume. ^{13}C spectra were either acquired on a Bruker AV 400 (9.4 T) or a Bruker DRX 500 (11.75 T). The 400 MHz instrument was equipped with a 10 mm broad band probe whereas the 500 MHz instrument was equipped with a 5 mm TXO $^1H/^{19}F/^{13}C$ triple resonance gradient inverse probe (^{19}F on the inner coil). All ^{13}C spectra taken at 400 MHz are ^1H decoupled, but since this particular variant of AV lacks triple resonance capabilities, all ^{13}C spectra acquired on this instrument were ^{19}F coupled. ^{13}C T_1's were measured at 400 MHz using the inverse recovery method,[25] and recycle delays were set approximately at 8 s from analysis of the results of this experiment. Chain end analyses were carried out on the 500 MHz instrument using approximately 1% solutions for ^1H and $^1H\{^{19}F\}$ acquisitions. ^1H, $^1H\{^{19}F\}$, and 2D $^1H-^{13}C$ heteronuclear single quantum coherence (HSQC) experiments with ^{19}F decoupling were also acquired on the 500 MHz system. It is important to note that during the course of the DEPT90 experiments, the TMS peak is not available for referencing. Also, referencing on the solvent, DMSO-d_6, is problematic since DEPT90[26] enhances the signal from the residual partially deuterated solvent, DMSO-d_5, which has a slightly different ^{13}C chemical shift from that of DMSO-d_6. Hence, all ^{13}C spectra were referenced to the $-CF_2H$ chain end peak at 113 ppm in both DEPT90 and $^{13}C\{^1H\}$ single pulse experiments, since this chemical shift is invariant regardless of the experiment used.

Rheology. Small amplitude oscillatory measurements were conducted to determine the complex viscosity and storage and loss moduli as a function of frequency at 230 °C. The instrument used is an ARES-LS strain-controlled rheometer equipped with 25 mm parallel plate geometry. All measurements were conducted under nitrogen atmosphere well within the linear viscoelastic regime.

Extensional viscosity measurements were conducted using the extensional viscosity fixture (EVF) hosted in the ARES-LS strain rheometer at 180 °C. Measurements were conducted at different extension rates ranging from 0.5 to 20 s^{-1}. The stress growth was recorded as a function of time and then converted into transient viscosity functions ($\eta_E^+(t)$). Additionally, step strain experiments were conducted in shear using parallel plate geometry to determine the terminal viscosity and the linear viscoelastic envelope (LVE)

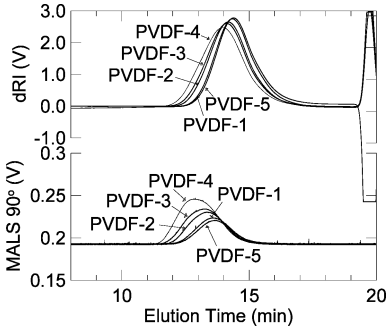

Figure 4. Raw detector voltages (top: differential refractometer, bottom: light scattering at 90°) measured for the reference samples in DMSO at 95 °C.

at 0.001 s^{-1}. This data was then converted into extensional viscosity using the Trouton's rule; $\eta_E^+ = 3\eta_0$.

Thermal Analysis. The melting point and heat of fusion were determined for all samples using a TAI Q1000 differential scanning calorimeter operating at 10 °C/min. The data were calculated during the second heating.

Results

The branching nature of the samples was investigated using several techniques including NMR, (SEC-MALLS), viscometry, and rheology. The combination of these methods provides a rugged and sensitive approach to detect the presence of LCB and obtain quantitative LCB level.

Table 2 shows the melting point, T_m, and the heat of fusion, ΔH, for the samples studied. The data shows that the melting point and the heat of fusion are slightly lower for the branched PVDF samples when compared to the reference ones. While the polymerization conditions can affect the final crystallinity and melting point, it is noteworthy that the ratio of reverse units, essentially controlled by the polymerization temperature, remains unchanged for the branched polymers compared to the reference samples. The differences observed in the DSC data are due to the presence of chain branching, which is known to affect the crystallinity.

SEC-MALLS-Viscosity. Molecular Weights. The molecular weight averages are given in Tables 3 and 4, which also provide the polydispersity index M_z/M_w. Cotts et al.[23] explained the reason for choosing M_z/M_w instead of M_w/M_n as the polydispersity index when using MALLS. The radius of gyration (weight average) is also given in these tables. The values of the molecular weights measured relative to a PMMA calibration were obtained using nine narrow polydispersity index PMMA standards. For the commercial samples, the relative molecular weights are between 1.6 and 1.8 times greater than the ones measured by light scattering. This is not a surprise since this method relies on the relationship between elution time and molecular size rather than with the actual molecular mass. For the experimental samples, the discrepancy between the absolute and the relative molecular weights is less pronounced. This difference is expected for samples featuring different architectures. This explanation is further detailed later.

The data in Tables 3 and 4 also point out the fact that the polydispersity indices for the experimental branched PVDF samples have broader distributions than the commercial ones. In fact, the chromatograms shown in Figure 5 indicate that the experimental samples are bimodal. The commercial samples also display some bimodality (Figure 4). As expected from the dependence of the intensity of the scattered light with the molar mass, it is in the light scattering traces that this bimodality is the most obvious. This bimodality is not strictly speaking one

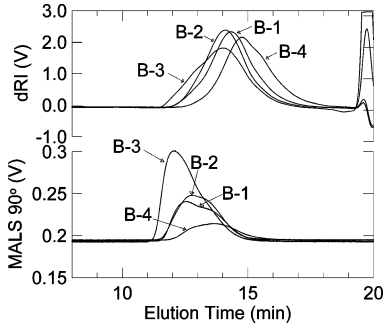

Figure 5. Raw detector voltages (top: differential refractometer, bottom: light scattering at 90°) measured for the experimental samples in DMSO at 95 °C.

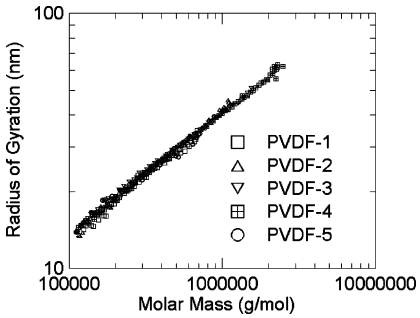

Figure 6. Radius of gyration R_G as a function of molar mass M for the reference samples measured in DMSO at 95 °C.

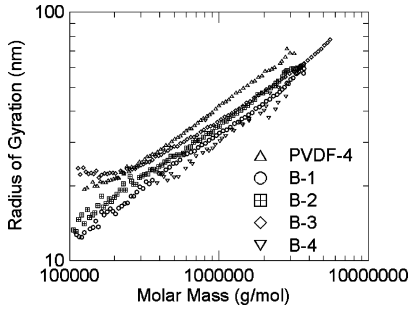

Figure 7. Radius of gyration R_G as a function of molar mass M for the experimental samples measured in DMSO at 95 °C. We also show one reference sample for comparison.

that pertains to a molecular weight difference but instead to a difference in branching density or architecture.

Radius of Gyration. The radius of gyration plots (R_G vs molar mass) for the commercial polymers are shown in Figure 6. The set of curves can be described as practically straight and overlapping lines. The noise level increases as the molar mass decreases, which is consistent with the loss of destructive interference as the size of the scattering object decreases. Because of this, the radius of gyration of the polymer with molecular weight below about 200 000 g/mol could not be measured. The data indicates that the five samples have similar architectures but differ in their respective molecular weight range.

Figure 7 shows the R_G vs molar mass curves for the experimental branched PVDF samples. Unlike in Figure 6, almost every sample seems to show a different behavior with the molar mass. Particular mention must be made about sample B-3. The R_G vs molar mass curve for this sample seems to loop back on itself. Such an anomalous behavior was described before for high-molecular weight branched polymers. Podzimek et al. reported it for randomly branched polystyrene.[27] Gerle et al.[28] reported it for PMMA brushes. It is explained by the delayed

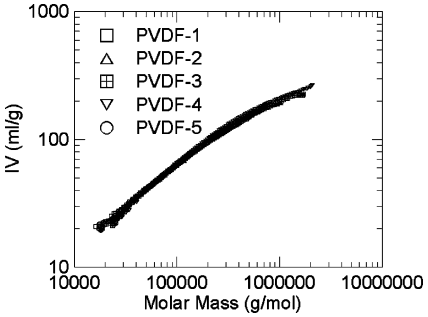

Figure 8. Intrinsic viscosity [η] as a function of molar mass M for the reference samples measured in DMSO at 95 °C.

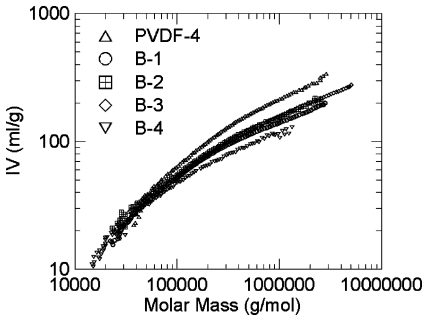

Figure 9. Intrinsic viscosity [η] as a function of molar mass M for the experimental samples measured in DMSO at 95 °C. We also show one reference sample for comparison.

Table 5. Values of the Mark−Houwink Exponent ν in the Relationship $R_G \propto M^{\nu}$

sample	exponent
PVDF-4	0.47
B-4	0.43
B-1	0.40
B-2	0.43
B-3	see text

elution of the high-molecular weight fraction of the polymer. The delayed high-molecular weight polymer elutes together with the low-molecular weight polymer whose elution time is not affected. As a result, at high retention times a mix enters the detectors consisting of low-molecular weight and high-molecular weight polymer. The radius of gyration is a *z*-average while the molecular weight is a weight average, which causes a distortion of the curve. The delayed elution is explained either by the "reptating" motion of the large polymer between the particles[28] or by the "anchoring" of the polymer in the pores.[27,28]

Sample B-4 has a relatively low molecular weight so we could measure a radius of gyration only for the high-molecular weight end of the distribution. This explains the higher noise level in the curve when compared to the other samples. Table 5 summarizes the value of the exponent ν in $R_G \propto M^{\nu}$ for the different samples. The rather large range of values reported in this table for ν indicates that the samples display different architectures.

Solution Viscosities. The Mark−Houwink plots for the commercial samples are shown in Figure 8. They confirm the findings of the previous section and indicate that for a given molecular weight, the chain architecture is essentially the same for all the samples in this series. One can see that the data for these samples are not linear in the log−log representation, which indicates some level of branching. This was further confirmed by the NMR and rheological data indicating a slight degree of branching. In the case of the experimental branched PVDF samples (Figure 9), the differences in the intrinsic viscosity are striking. This reflects the changes in the architecture of these

Table 6. Concentration of $-CF_2CH(CF_2-)CH_2-$ Methines /1000 Repeat Units

sample	no. of methines
B-4	4.8
B-1	4.0
B-2	4.0
B-3	4.6
PVDF-1	1.0
PVDF-2	1.1
PVDF-3	1.9
PVDF-4	3.1

samples. In addition, the data confirm that there are two regions for the samples with a higher branching density for high molecular weight.

From all the samples, B-4 is the most branched followed by B-1, B-2, B-3, and PVDF-4. Note that sample B-3 does not display the characteristic shape it showed in the radius of gyration curves. This is because the $[\eta]$ is a viscosity average while R_G is a *z*-average number. The viscosity average is close to a weight average.

NMR Results. While several side reactions can occur during the course of polymerization, which could lead to branching, the suggested mechanism in our particular case is through chain transfer. Indeed, a carbon radical can be moved from one location to another by an intermolecular or intramolecular hydrogen atom transfer, which in some cases results in branching. For example, in the case of styrene or methacrylate monomers, graft site formation is due to initiator radical attack onto the backbone via allylic hydrogen abstraction. Significant levels of grafting are achieved and depend upon the relative concentrations of monomer and backbone polymer but not upon the level of initiator. For acrylic monomer, graft site formation was found to be due to polymer radical attack at the double bond in the backbone.[29]

Recently Apostolo et al.[30] proposed short chain branching from backbiting, where both of their reaction mechanisms go through an intramolecular five- membered ring transition state. They also proposed long chain branching from radicals reacting with terminal double bonds, $R^\bullet + RCH{=}CF_2 \rightarrow RC^\bullet HR$, or chain transfer to the polymer, $RCH_2CF_2^\bullet + RCH_2R \rightarrow RCH_2$-$CF_2H + RC^\bullet HR$. In both cases, a mathematical model based on the chain end concentration and SEC curve was developed to quantify each. In our approach, the NMR data gives direct evidence of the branching. In our particular case, we suspect that grafting could be generated by abstraction of hydrogen from the polymer backbone by a radical. This could either be a persulfate radical or a radical generated by Luperox 230. Furthermore, branching in poly(vinylidene fluoride), by its very nature, must exhibit either fluoromethine or methine moieties, i.e., $>CF-$ or $>CH-$, respectively. The first of these, the fluoromethine, would exhibit a peak, or peaks, between 75 and 90 ppm in the ^{13}C NMR spectrum[31] [For example, the^{13}C spectrum of PVDF/HFP shows the fluoromethine at 90 ppm], and peaks upfield of -150 ppm in the ^{19}F spectra.[32] No fluoromethines were observed in these regions even when acquisitions were carried out that yielded detection levels of 1 branch point per 1000 repeat units or less, hence ^{19}F NMR eliminates fluoromethines as possible branch points. However, several methines were detected using the DEPT90 pulse sequence (see Table 6).[26,33] DEPT90 enhances any signals from methine carbons and negates spectral overlap by suppressing any methyl, methylene, as well as any carbon peaks without any directly bound hydrogens. e.g., $-CO_2-$, $-OCO_2-$, $-CF_2-$ peaks. Figure 10 shows the result of the most highly branched

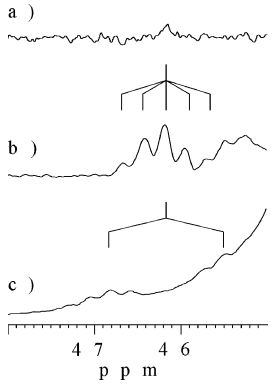

Figure 10. ^{13}C spectra of sample B-4 (a) both ^1H and ^{19}F decoupled, single pulse, (b) DEPT90 ^1H decoupled, (c) DEPT90 fully coupled, in DMSO-d_6, at 80 °C.

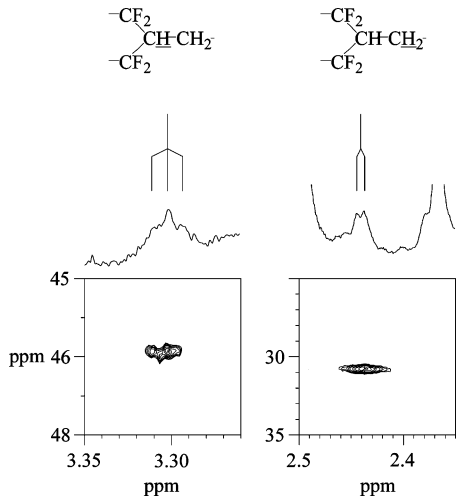

Figure 11. ^{19}F fully decoupled $^1H/^{13}C$ HSQC spectrum of sample B-4 (a) branching methine region, (b) methylene α to the branching methine region, in DMSO-d_6, at 80 °C.

sample: sample B-4. The peak at 46 ppm is assigned to a methine carbon in the PVDF chain. Other methines observed in the DEPT90 spectrum can be assigned to chain ends (The most predominant of these chain ends is the hydrogen abstraction chain end, $-CF_2H$, which has a ^{13}C chemical shift of 113 ppm.) and the residual partially deuterated component of the solvent, DMSO-d_5. The coupling patterns for the branch point indicate that the methine has four equivalent, or nearly chemically equivalent, fluorines on carbons α to the methine. The coupling constant magnitudes are as follows $^1J_{CH}$ (observed) = 134 Hz (doublet) from ^1H coupled DEPT90 experiments and $^2J_{CF}$ (observed) = 24.2 Hz quintet from ^1H decoupled DEPT90 experiments, Figure 10. Also, to confirm that the peak at 46 ppm was not from two overlapping ^{13}C peaks, a single pulse ^{13}C with simultaneous ^1H and ^{19}F decoupling experiment was carried out. Since the C−F coupling pattern and vinylidene fluoride structure constrains the methine to be connected to two $-CF_2-$'s, then the third leg in the branch point must be a $-CH_2-$, as is demonstrated in the ^{19}F decoupled $^1H/^{13}C$ HSQC,[34] $^1H\{^{19}F\}$ homonuclear decoupling,[35] and selective $^1H\{^{19}F\}$ COSY experiments,[36] see Figures 11 and 12. The HSQC shows that the methine proton of the branch point has a chemical shift of 3.2 ppm, and it exhibits the requisite $^3J_{HH}$ triplet coupling (J_{obs} = 3.7 Hz) in single pulse $^1H\{^{19}F\}$ experiments, proving that the adjacent group on the third leg is indeed a $-CH_2-$. This third leg $-CH_2-$ was assigned using ^1H homonuclear decoupling, Figure 12, and selective COSY experiments, both conducted under ^{19}F decoupling. Performing both of these

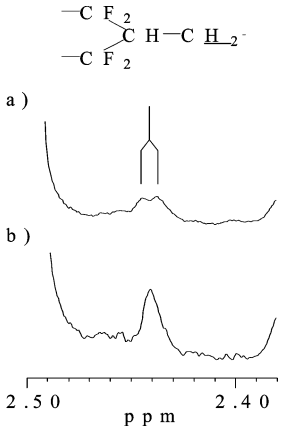

Figure 12. ^{19}F fully decoupled ^{1}H spectra (a) no homonuclear decoupling, (b) homonuclear decoupling with the decoupler set at 3.2 ppm, the chemical shift of the branching methine proton, in DMSO-d_6, at 80 °C.

redundant experiments was required to ensure correct assignments for these low signal-to-noise peaks. The ^{1}H chemical shift of the $-CH_2-$ adjacent to the methine branch point is at 2.45 ppm and displays the requisite $^{3}J_{HH}$ doublet coupling pattern (J_{obs} = 3.7 Hz). In reference back to the HSQC experiment, Figure 11, the ^{13}C chemical shift of this third leg $-CH_2-$ comes at 30.75 ppm. For branch point detection and quantification, ^{19}F provides insight and would be a useful tool for quantification. However, it appears that the two fluoromethylene groups adjacent to the branch point methine overlap with the −92 ppm peak caused by reverse units. This assignment was made by acquiring a ^{19}F spectrum and performing selective ^{1}H decoupling on the methine proton of the branch point. Under these conditions the $^{3}J_{HF}$ couplings between the branch point methine and the adjacent fluorines should be negated. Upon close comparison of the ^{1}H coupled and ^{1}H selectively decoupled ^{19}F spectra, the only detectable difference was a simplification of the multiplicities on the −91.93 ppm peak. Hence the two fluoromethylenes adjacent to the branch point methine were assigned to this chemical shift.

To summarize, all the NMR data is consistent with the structure of the branch point shown below:

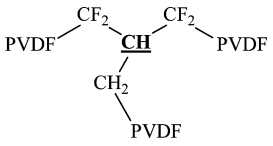

This structure is not consistent with a methine resulting from backbiting.[30,37] Backbiting is thought to occur from a 1,5 intramolecular shift with a hydrogen abstraction at a $-CH_2-$ of a "head-to-head" site, proposed scheme shown below.

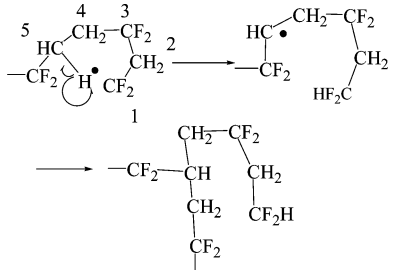

The presence of 1,4 and 1,6 intramolecular shifts in an isoregically propagating chain would result in the $-CF_2^{\bullet}$ chain end forming a transition state with a five- or seven-membered ring to abstract hydrogen. This is not as probable as the six-membered ring shown above. Also, a methine formed in this backbiting mechanism should show a ^{13}C chemical shift upfield from the isoregic carbon peak,[38] and its coupling pattern would show a $^{2}J_{CF}$ triplet instead of the observed quintet, Figure 10. The $-CF_2^{\bullet}$ chain end could abstract a hydrogen from many sources, but backbiting would certainly contribute to the concentration of $-CF_2H$ chain ends. There does not appear to be a correlation between $-CF_2H$ chain end concentration and branch point concentration, see Table 7. Also, the proposed mechanism indicates that backbiting should correlate with the concentration of reverse units. There does not appear to be a correlation between reverse unit concentration and branch point concentration either, see Table 8.

Table 7. Concentration of Hydrogen Abstraction Chain Ends/1000 Repeat Units via ^{1}H NMR

sample	CF_2H	CF_2CH_3
PVDF-1	1.0	1.1
PVDF-2	1.0	1.1
PVDF-3	0.8	1.0
PVDF-4	0.9	1.1
B-4	6.2	5.1
B-1	4.0	3.8
B-2	3.7	3.3
B-3	2.4	1.6

Table 8. Concentration of Reverse Units in PVDF Chains via ^{19}F NMR

sample	reverse units (%)
B-4	5.9
B-1	5.6
B-2	5.7
B-3	5.7
PVDF-2	4.9
PVDF-3	5.0
PVDF-4	4.9
PVDF-5	4.9

Also, reference should be made to previous attempts at finding branch points in the ^{19}F spectra. Lutringer et. al[24] used Cais and Sloane's[39] statistical treatment of the VF_2 additions to find an inconsistency large enough to ascribe to branch points. They assigned the branched points in the ^{19}F spectrum but could not decide whether these peaks were from statistical inconsistencies, could be ascribed to branch points, or due to impurities in the polymer. ^{19}F spectral with and without selective ^{1}H decoupling at 3.2 ppm show that the −91.93 ppm peaks are the most likely candidates for the two $-CF_2-$'s adjacent to the $>CH-$. Considering the region that Lutringer focused on, −113 to −115 ppm, selective ^{1}H decoupling experiments did not allow a conclusive assignment of the $>CHCH_2CF_2$-fluorine.

In some samples, two types of methines were observed. The first type, the dominant branching species, has already been discussed (^{1}H δ = 3.2 ppm and ^{13}C δ = 46 ppm), and its structure illustrated above. HSQC experiments indicated that the second type of methine, or branch point, has the following chemical shifts, ^{1}H δ = 3.35 ppm and ^{13}C δ = 47 ppm and its concentration never exceeded that of the first type by more than a factor of 0.25. TOCSY experiments indicate that the local environment about the methine of this second type is asymmetric, i.e., that the methine is chiral. Because of the extreme dilution of this second type, it is difficult to refine its structure but the structure is consistent with a branch point adjacent to a reverse unit giving a local structure of the form $-CH_2CF_2CH-(CH_2-)CF_2CF_2-$. While this structure does not support a

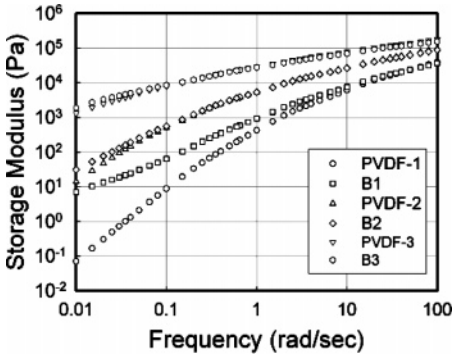

Figure 13. Storage modulus versus frequency of the reference and branched PVDF samples at 230 °C.

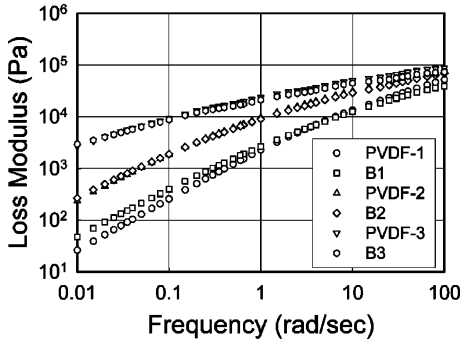

Figure 14. Loss modulus as a function of frequency of the reference and branched PVDF samples at 230 °C.

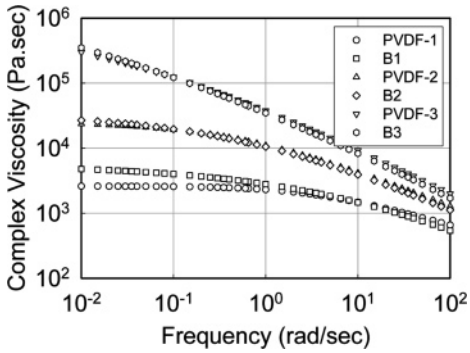

Figure 15. Complex viscosity as a function of frequency of the reference and branched PVDF samples at 230 °C.

traditional backbiting scheme, it does provide evidence for multiple branching mechanisms.

Rheology Results. Shear rheology in the oscillatory mode was used to assess the viscoelastic properties of selected reference samples and the branched PVDF. The sample selection is based on identical viscosities, therefore only those pairs which are comparable in viscosity are discussed here and shown in Figures 13−15.

Figure 13 shows the storage modulus (G') versus frequency at 230 °C. The results are also compared to corresponding reference samples for different molecular weights. The low molecular weight reference sample showed a typical profile common with most linear polymers. As the molecular weight is increased, the terminal zone where $G' \sim \omega^2$ is shifted to lower frequencies as a result of longer chains and a broader molecular weight distribution. For the branched PVDF samples, the storage modulus appears to be identical to their reference counterparts at high frequencies. However, in the terminal region, there exists a deviation from the reference samples. The extent of this deviation is related to the sensitivity of the rheological properties to chain branching and to the formation of a high-molecular weight population. For the lower-molecular weight sample (B-1), the deviation is the largest and the presence of chain branching significantly increases the modulus suggesting a much longer relaxation time than that of its equivalent reference sample (PVDF-1). As the molecular weight is increased, there is a competition between the high-molecular weight chains and chain branching in that both exhibit a longer relaxation time. It also appears that the enhancement in the modulus is molecular weight dependent. This is not necessarily reflecting the amount of branching but rather shows that the branching effect for higher molecular weight samples is hidden by the high-molecular weight fraction in this sample. The branching effect is better observed with the lowest-molecular weight sample. These changes in the relaxation time and modulus are typical of branched polymers and have been reported for other polymers such as polystyrene and polyethylenes.[40,41]

Figure 14 shows the loss modulus as a function of frequency for reference samples as well as the branched ones. The trend in the loss modulus follows, to some extent, that of the viscosity in that the frequency dependence of the branched samples is almost identical to the reference samples. However, the same difference is observed for the low-viscosity couple. These results are supportive of the idea that the viscous components among these sample pairs remain unchanged and allow their melt processing under similar conditions.

Figure 15 shows the complex viscosity versus frequency at 230 °C for the branched samples as compared to the reference samples. The viscosity profiles of the samples, in the frequency range studied, are reflective of their architecture. The weight average molecular weight (M_w) is correlated to the zero-shear viscosity following the Rouse model $\eta \sim M_w^{3.4}$. The molecular weight distribution is typically correlated to the breadth of the transition between the Newtonian plateau and the pseudo-plastic region, while chain branching affects both the terminal region and the non-Newtonian region. While the Newtonian plateau is not achieved for all the samples except for the lowest-molecular weight pair, it is clearly shown that the branched PVDF tends toward a higher zero-shear viscosity than the reference counterparts. This is in agreement with the fact that branched polymers possess a higher zero-shear viscosity than linear polymers.[42,43] In the transition between the Newtonian plateau and the high-frequency region, a crossover point is observed in all three pairs and is also another indication of a change in the dynamics of the polymer chains. The onset of shear thinning is reduced to lower frequency while the shear thinning behavior remains almost identical. However, it is difficult to make a rigorous assessment of the chain branching effect due to the changes in molecular weight distribution associated with the polymerization process.

Despite the difficulty of the experimental procedure, one of the most sensitive techniques to detect long chain branching is extensional viscosity. Recently, Sentnamat introduced a rather simple design of an extensional fixture that can be used in shear rheometers having excellent oven temperature control.[44,45] This new fixture allows transient measurements in extensional flows up to a Hencky strain of 4. Figures 16−18 show the extensional viscosity of the reference samples at extension rates of 0.5, 1, 5, and 20 s^{-1} and a temperature of 180 °C. In each plot the results of the stress growth experiments were added following $\eta_E^+ = 3\eta_0$. For each sample, the LVE envelope indicates the

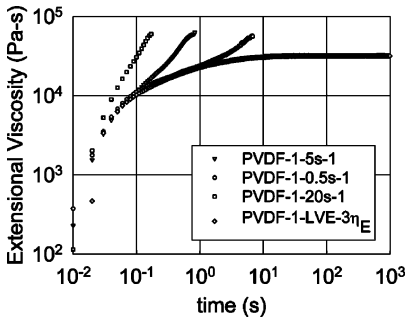

Figure 16. Extensional viscosity of reference sample PVDF-1 at 180 °C and extension rates of 0.5, 5, and 20 s^{-1}. Stress growth experiment conducted at a rate of 0.03 s^{-1}. LVE is calculated using Trouton's rule.

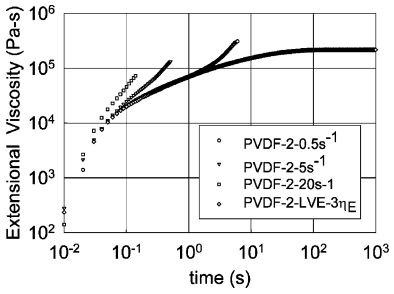

Figure 17. Extensional viscosity of reference sample PVDF-2 at 180 °C and extension rates of 0.5, 5, and 20 s^{-1}. Stress growth experiment conducted at a rate of 0.02 s^{-1}. LVE is calculated using Trouton's rule.

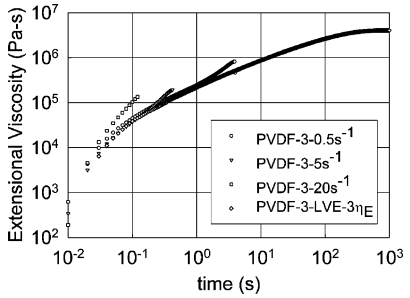

Figure 18. Extensional viscosity of reference sample PVDF-3 at 180 °C and extension rates of 0.5, 5, and 20 s^{-1}. Stress growth experiment conducted at a rate of 0.004 s^{-1}. LVE is calculated using Trouton's rule.

steady-state viscosity in the Newtonian region. For the extensional viscosity measurements, it is possible to observe a slight deviation from the LVE envelope as the extension rate is increased. These deviations are referred to as strain hardening and are representative of a second relaxation time, which may be associated with chain branching or molecular weight distribution. These results suggest that while the reference samples have identical polydispersity indexes ($M_w/M_n \sim 2-3$), the strain hardening observed could be related to the presence of small fractions of branched chains.[46,47] Figures 19−21 show the transient measurements $\eta_E^+ = f(t)$ for the experimental samples at 180 °C and for identical extension rates. In this case, the LVE envelopes were obtained at much lower shear rates to be able to achieve the Newtonian plateau. For the extensional viscosity measurements, the deviation from the LVE envelope is much more significant and clearly reflects the presence of chain branching as indicated in similar studies.[48,49]

Discussion

It is well-known that there is a distinct relationship between polymer architecture and rheology. The molecular weight,

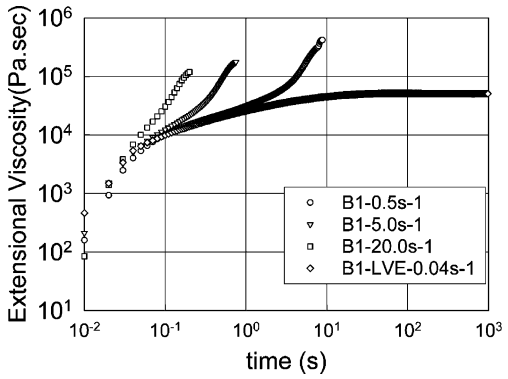

Figure 19. Extensional viscosity of branched PVDF B-1 at 180 °C and extension rates of 0.5, 5, and 20 s^{-1}. Stress growth experiment conducted at a rate of 0.05 s^{-1}. LVE is calculated using Trouton's rule.

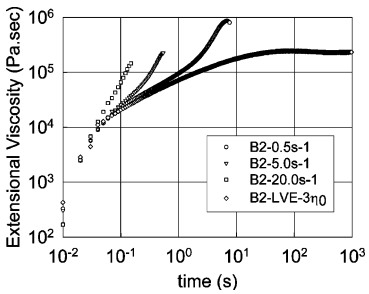

Figure 20. Extensional viscosity of branched PVDF B-2 at 180 °C and extension rates of 0.5, 5, and 20 s^{-1}. Stress growth experiment conducted at a rate of 0.005 s^{-1}. LVE is calculated using Trouton's rule.

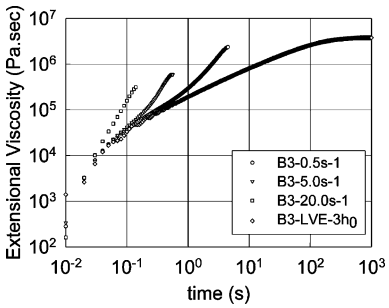

Figure 21. Extensional viscosity of branched PVDF B-3 at 180 °C and extension rates of 0.5, 5, and 20 s^{-1}. Stress growth experiment conducted at a rate of 0.002 s^{-1}. LVE is calculated using Trouton's rule.

molecular weight distribution, and chain branching have a strong effect on the rheological behavior of polymers. This is certainly the case for polyolefins and more specifically metallocene polyethylenes.[5] In the present study, the reference samples were produced by a commercial process and contain a fraction of high molecular weight with long chain branches that are inherent to this type of process. It is therefore recognized that the reference samples are not purely linear polymers. On the other hand, the experimental samples were produced by a similar process but where the presence of a coinitiator such as Luperox 230 and the synthesis conditions promote the formation of long chain branches. While the type of branches and their structure is not well understood yet, the branch points are believed to be randomly distributed and nonuniform in the number of repeat units. This is a necessary and sufficient condition to achieve the desired rheological properties.

With SEC/MALLS/VISCO, the presence of branches was demonstrated in both the commercial and experimental samples. NMR confirmed that these branches were covalently bonded

and not of physical nature as suggested by Lutringer et al. .[50] The quantification of the branches was also possible by NMR. We make no attempts at quantifying the level of branches using the MALLS or viscosity data because this requires purely linear samples and we have shown that even the reference samples comprise a significant amount of branched species. The data indicate that while branching in the commercial samples is only present at the high-molecular weight fraction, it is a feature consistently present across the entire molecular weight distribution for all the experimental branched samples in this study. The experimental samples were found to be overall more branched than the commercial reference samples, over the entire molecular weight distribution range. However, branching density is not uniform as it increases with molecular weight.

It is worth discussing the data in Tables 3 and 4 since they can be interpreted in terms of architecture. Using the data obtained for the low-molar mass portion of the sample displaying less branching and assuming that in this region the polymer is essentially linear, we can now compare the Mark−Houwink coefficients of PVDF to the coefficient for PMMA.[51] The values are summarized here

$$\text{PVDF:}\quad [\eta]_{\text{PVDF,95°C}} = 0.01511M^{0.73}$$

$$\text{PMMA:}\quad [\eta]_{\text{PMMA,95°C}} = 0.01121M^{0.68}$$

Lutringer et al.[50] reported an exponent α of 0.70 for PVDF in good solvents. Note that Lutringer's values are the result of measurements made on individual broad samples and average values were used for the molar mass and [η].

From these two relationships, it is clear that at a given molecular weight, the intrinsic viscosity and thus the molecular dimension of a PMMA polymer will be significantly smaller than a PVDF polymer. This means that at a given elution time, a PMMA polymer will have a higher molecular weight than a PVDF eluting at the same time. As a result, when one uses a PMMA calibration to determine the molecular weight of PVDF, one will overestimate the molecular weight of the PVDF. When the PVDF is branched, the first relationship above is not valid anymore, and because of the more compact structure, the elution time of the branched PVDF will become closer to that of the linear PMMA.

The effect of long chain branching is clearly seen in the storage modulus measurement. There exists a qualitative correlation between the number of branches in a given sample and the enhancement in the modulus at low frequencies. While the experimental samples have a higher molecular weight than their reference counterparts, they however display a similar storage modulus dependence on frequency. For example, the molecular weights of samples B-2 and PVDF-2 are quite different (260 000 and 162 000, respectively) but their storage moduli, as well as the viscosity curves, are identical. One implication in terms of polymer processing is that it would be easier to melt process such polymers even if they have a high molecular weight. For the lower viscosity samples, the difference in the storage modulus is significant in that the enhancement in the low-frequency region is strongly dependent on branching but also on the higher value of M_z compared to the reference sample. Overall, all experimental branched samples studied here show a larger value of M_z. The experimental samples are overall more branched than the commercial reference samples over the entire molecular weight distribution range. Each sample displays a distribution of branching density, with the high-molecular weight fraction being more branched. As a result, the rheological properties become dependent on both parameters, i.e., branching and molecular weight distribution.

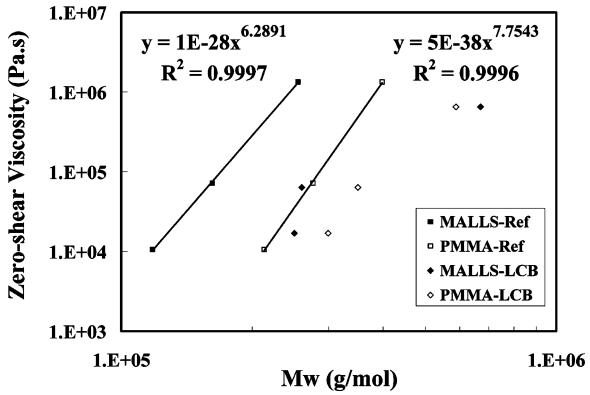

Figure 22. Zero-shear viscosity correlation with average molecular weight of the reference and branched PVDF samples. Zero-shear viscosity determined by stress growth experiments at 180 °C. SEC data shown is by standard PMMA calibration as well as light scattering techniques.

With the use of the values of the zero-shear viscosity as determined by the stress growth experiments, it is possible to examine the classical correlation between the viscosity and molecular weight. Though more data points would be preferred, it is still possible to compare the results between the reference samples and the branched samples. Figure 22 shows the correlation between the zero-shear viscosity and molecular weight measured by MALLS and by the standard PMMA calibration methods. The linear fit on a log−log scale shows a slope of 6.3 for the reference samples based on MALLS data and 7.8 based on the PMMA calibration curve. Those values are much larger than the theoretical and experimental value of 3.4 observed for many linear polymers. Such a behavior has been observed for PVDF by many authors[52,53] and explained by a combination of small fractions of branched chains as well as the presence of a strong dipole moment responsible for a stiffening of the backbone, which would lead to a rodlike polymer behavior. Such deviations from the 3.4 exponent have been discussed in the literature and shown for branched polymers, rodlike polymers, and ionomers. This correlation appears to be identical for both MW determination techniques with a shift in the *x*-axis reflecting the correction based on the PMMA calibration. The branched samples appear to have a lower zero-shear viscosity than the reference samples for an identical molecular weight in the range studied. The shift in the zero-shear viscosity is quite significant (an order of magnitude). Results from the literature indicate similar findings for polyethylenes though the deviations are more reasonable. Indeed, when a small amount of long chain branching is present in metallocene linear low-density polyethylene, mLLDPE, an increase in the zero-shear viscosity is observed over the linear counterpart with similar molecular weight. This is mainly due to the change in the radius of gyration, which becomes smaller for the branched sample as indicated in the light scattering data. However, when the amount of chain branching increases with molecular weight, the zero-shear viscosity is lower than the linear samples.[3,54,55] These results are in agreement with our findings in that the amount of long chain branching contained in PVDF is large enough to cause a drop in the zero-shear viscosity below the threshold line of the reference samples. It is noteworthy to mention that even for the reference samples, the presence of small amounts of chain branching yields a relative shift of the correlation with respect to the branched ones. This has been shown in the extensional viscosity measurement

showing a slight degree of strain hardening for all reference samples.

Finally, it is worth mentioning that the process developed to introduce branching in the PVDF chain also allows controlling its level. As one can see, sample B-4 displays the highest level of branching, both by NMR analysis and by MALLS analysis. The resulting molecular weight however was much lower probably because the Luperox 230 initiator can also generate transfer. Therefore, the rheology profile could not be fully investigated. The NMR spectrum for this sample clearly shows a higher concentration of chain ends confirming MALLS low-molecular weight data (see Tables 6 and 7).

Conclusion

This paper conclusively demonstrates that long chain branching naturally occurs in emulsion polymerized PVDF. Our results indicate that the production of LCBs appears to be consistent with a mechanism requiring hydrogen abstraction from the backbone. Once the synthetic methodology and rationalization was established, we focused on the unique properties of these highly branched PVDF. Many of the rheological properties of these new polymers indicate that they would be suitable for new applications in melt processing.

PVDF featuring long chain branches was synthesized using potassium persulfate and *n*-butyl-4,4-bis(*tert*-butylperoxy) valerate (Luperox 230). The number of branch points per 1000 monomer units for the experimental samples was determined by NMR to be in the range 4.0−4.8 while for reference PVDF this number ranged between 0.8 and 3.1. Increasing the amount of Luperox 230 had the effect of increasing the number of branch points, and this resulted in a more compact and branched polymer as indicated by the MALLS and viscometry data. The proposed mechanism for the formation of these branches is hydrogen abstraction from the polymer backbone. These results offer an unprecedented opportunity to tailor the microstructure of these polymers and subsequently their physical properties.

The key rheological parameters investigated gave us a good overall picture of the structure−property relationship in these polymers. By analogy to what was previously reported in the literature for other branched polymers such as in polyolefins, we found that PVDF containing long chain branching exhibits similar behavior and overall rheological properties. For instance branched polymers may possess a lower or higher zero-shear viscosity than linear counterparts depending on the amount of LCB in the polymer, while in both cases they display a lower onset of shear thinning than reference samples.

The zero shear viscosity for the reference PVDF samples was found to correlate with the weight-average molecular weight to the 6.3 power for MALLS data and 7.8 based on the PMMA calibration curve. This value, higher than 3.4 typically observed for many linear polymers, is however not unusual for PVDF and has been reported elsewhere. Nonetheless, the branched samples studied appear to have a lower zero-shear viscosity than the reference samples for an identical molecular weight in the range studied.

Furthermore, by examining the shear and extensional rheological properties for these LCB PVDF we found that the presence of long-chain branching had a direct impact on uniaxial extensional viscosity, where they exhibited strain hardening in a wide range of extension rates ($0.5-20.0\ s^{-1}$),

While this work allowed for a thorough characterization of these branched polymers, many questions remain. For example, it would be interesting to further understand and separate the effects coming from the branching structure from those of branching density.

References and Notes

(1) Graessley, W.W. Viscoelasticity and Flow in Polymer Melts and Solutions. In *Physical Properties of Polymers*, 2nd ed.; American Chemical Society: Washington, DC, 1984; p 97.
(2) Munstedt, H.; Steffi, T.; Malmberg, A. *Rheol. Acta* **2005**, *45*, 14.
(3) Gabriel, C.; Munstedt, H. *Rheol. Acta* **2002**, *41*, 232.
(4) Wood-Adams, P.; Dealy, J. M.; Degroot, A. W.; Redwine, O. D. *Macromolecules* **2000**, *33*, 7489.
(5) Malmberg, A.; Gabriel, C.; Steffi, T.; Munstedt, H.; Lofgren, B. *Macromolecules* **2002**, *35*, 1038.
(6) Mekhilef N.; Pasquariello, G. O. Proceedings of the SPE/ANTEC Conference, Charlotte, NC, May 7−11, 2006.
(7) Sperber, O.; Kaminsky, W. *Macromolecules* **2003**, *36*, 9014−9019.
(8) Loontjens, J.A.; Plum, B. J. M. Process for Preparing a Branched Polymer. Patent WO/2001/066617, September 13, 2001.
(9) Menges, M. G.; Schmidt-Rohr, K.; Penelle, J. *Polym. Prepr.* (224th ACS National Meeting; Polymer Chemistry) **2002**, *43* (2), 472−473.
(10) Weng, W.; Markel, E. J.; Dekmezian, A. H. *Macromol. Rapid Commun.* **2001**, *22*, 1488−1492.
(11) Qui, W.; Pyda, M.; Nowak-Pyda, E.; Habenschuss, A.; Wagener, K. B.; Wunderlich, B. *J. Polym. Sci., Part B: Polym. Phys.* **2006**, *44*, 3461.
(12) Santangelo, P. G.; Roland, C. M.; Puskas, J. E. *Macromolecules* **1999**, *32*, 1972.
(13) Shroff, R. N.; Mavridis, H. *Macromolecules* **1999**, *32*, 8454−8464.
(14) Lee, J. H.; Archer, L. A. *Macromolecules* **2002**, *35*, 6687−6696.
(15) Graebliong, D. *Macromolecules* **2002**, *35*, 4602−4610.
(16) Auhl, D.; Stange, J.; Münstedt, H.; Krause, B.; Voigt, D.; Lederer, A.; Lappan, U.; Lunkwitz, K. *Macromolecules* **2004**, *37*, 9465−9472.
(17) Maccone, P.; Apostolo, M.; Ajroldi, G. *Macromolecules* **2000**, *33*, 1656−1663.
(18) Apostolo, M.; Biressi, G. *Macromol. Symp.* **2004**, *206*, 347−360.
(19) Arcella, V.; Brinati G.; Albano M.; Tortelli V. Fluoroelastomers Comprising Monomeric Units Derving from a Bis-Olefin. U.S. Patent 5,585,449, December 17, 1996.
(20) Amos, S. E.; Hintzer, K.; Kaspar, H.; Lavallee, C. Melt-Processible Polymer Composition Comprising Fluorpolymer Having Long Chain Branches. U.S. Patent Appl. 20040260022 A1, December 23, 2004.
(21) Hedhli, L.; Mekhilef Arkema, N. Branched Fluoropolymers, U.S. Patent Appl. 20070106010, May 10, 2007.
(22) Tsierkezos N. G.; Kalarakis A. E.; Palaiologou M. M. *J. Chem. Eng. Data* **2000**, *45*, 395−398.
(23) Cotts, P. M.; Guan, Z.; McCord, E.; McLain, S. *Macromolecules* **2000**, *33*, 6945−6952.
(24) Lutringer G., Weill G. *Polymer* **1991**, *32*, 877.
(25) Farrar, T. C.; Becker, E. D. In *Pulse Fourier Transform NMR. Introduction to Theory and Methods*; Academic Press: New York, 1971.
(26) Doddrell, D. M.; Pegg, D. T.; Bendall, M. R. *J. Magn. Reson.* **1982**, *48*, 323.
(27) Podzimek, S.; Vlcek, T.; Johann, C. *J. Appl. Polym. Sci.* **2001**, *81*, 1588−1594.
(28) Gerle, M.; Fischer, K.; Roos, S.; Müller, A. H. E.; Schmidt, M.; Sheiko, S. S.; Prokhotova, S.; Möller, M. *Macromolecules* **1999**, *32*, 2629−2637.
(29) Huang, N. J.; Sundberg, D. *J. Polym. Sci., Part A: Polym. Chem.* **1995**, *33*, 2571.
(30) Apostolo, M.; Arcella, V.; Storti, G.; Morbidelli, M. *Macromolecules* **1999**, *32*, 989−1003.
(31) Tonelli, A. E.; Schilling, F. C.; Cais, R. E. *Macromolecules* **1981**, *14*, 560−564.
(32) Schmiegel, W.W. *Angew. Makromol. Chem.* **1979**, *76*/*77*, 39−65. Majumdar, R. N.; Harwood, H. J. In *Applied Polymer Analysis and Characterization*; Mitchell, J., Jr., Ed; Hanser: New York, 1980; Chapter III-G.
(33) Bendall, M. R.; Doddrell, D. M.; Pegg, D. T. *J. Am. Chem. Soc.* **1981**, *103*, 4603.
(34) Bodenhausen, G.; Ruben, D. J. *Chem. Phys. Lett.* **1980**, *69*, 185−189.
(35) Anderson, W. A.; Freeman, R. *J. Chem. Phys.* **1962**, *37*, 85−103.
(36) Bauer, C.; Freeman, R.; Frenkiel, T.; Keeler, J.; Shaka, A. J. *J. Magn. Reson.* **1984**, *58*, 442−457.
(37) Pianca, M.; Barchiesi, E.; Esposito, G.; Radice, S. *J. Fluorine Chem.* **1999**, *95*, 71−84.
(38) Tonelli, A. E.; Schilling, F. C.; Cais, R. E. *Macromolecules* **1981**, *14*, 560.
(39) Cais, R. E.; Sloane, N. J. A. *Polymer* **1983**, *179*, 24.
(40) Hepperle, J.; Munstedt, H.; Haug, P. K.; Eisenbach, C. D. *Rheol. Acta* **2005**, *45*, 151−163.

(41) Van Ruymbeke, E.; Stéphenne, V.; Doust, D.; Godard, P.; Keunings, R.; Bailly, C. *J. Rheol.* **2005**, *49*, 1503.
(42) Sammler, R. L.; Karjala, T. P.; Huang, W.; Mangnus, M. A.; Hazlitt, L. G.; Johnson, M. S. Proceedings of SPE/ANTEC Conference, Chicago, IL, May 16−20, 2004; p 1023.
(43) Sammler, R. L.; Karjala, T. P.; Huang, W.; Mangnus, M. A.; Hazlitt, L. G.; Johnson, M. S. Proceedings of SPE/ANTEC Conference, Chicago, IL, May 16−20, 2004; p 1018
(44) Sentmanat, M. L., Wang B. N.; McKinley G. *J. Rheol.* **2005**, *49*, 585.
(45) Sentmanat, M. L. *Rheol. Acta* **2004**, *43*, 657.
(46) Munstedt, H. *J. Rheol.* **1980**, *24*, 847.
(47) Trzebiatkowski, T.; Wilski, H. *Rheol. Acta* **1985**, *24*, 582.
(48) Gabriel, C.; Munstedt, H. *J. Rheol.* **2003**, *47*, 619−630.
(49) Wagner, M. H.; Bastian, H.; Bernat, A.; Kurzbeck, S.; Chai, C. K. *Rheol. Acta* **2002**, *41*, 316−325.
(50) Lutringer, G.; Meurer, B.; Weill, G. *Polymer* **1991**, *32* (5), 884.
(51) Moyses, S., to be published.
(52) Mekhilef, N.; Pattamaprom, C.; Rondeau, E. Presented at the 74th Annual Meeting of the Society of Rheology, Minneapolis, MN, October 13−17, 2002.
(53) Carrot, C.; Guillet, J.; May, J.-F. *Makromol. Chem., Macromol. Symp.* **1989**, *23*, 113−119.
(54) Graessley, W. W.; Masuda, T.; Roovers, J. E. L.; Hadjichristidis, N. *Macromolecules* **1976**, *9*(1), 127.
(55) Janzen, J.; Colby, R. H. *J. Mol. Struct.* **1999**, *485−486*, 569−584.

MA071160Z